Available online at www.sciencedirect.com
ScienceDirect
Journal of Sound and Vibration 324 (2009) 57–73
JOURNAL OF SOUND AND VIBRATION
www.elsevier.com/locate/jsvi

Decomposition of modal acoustic power due to cascade–turbulence interaction

Cheolung Cheong[a,*], Vincent Jurdic[b], Phillip Joseph[b]

[a]*School of Mechanical Engineering, Pusan National University, 30, Jangjeon-dong, Guemjeong-gu, Pusan 609-735, Republic of Korea*
[b]*Institute of Sound and Vibration Research, University of Southampton, Highfield, Southampton SO17 1BJ, UK*

Received 7 May 2008; received in revised form 3 November 2008; accepted 31 January 2009
Handling Editor: L.G. Tham
Available online 13 March 2009

Abstract

This paper investigates the modal acoustic power (MAP) generated by a cascade of flat-plate airfoils interacting with homogeneous, isotropic turbulence. The basic formulation for the upstream and downstream acoustic power based on the analytical theory of Smith [Discrete frequency sound generation in axial flow turbomachines, Reports and Memoranda no. 3709, Aeronautical Research Council, 1972] and its generalization to broadband noise due to Cheong et al. [High frequency formulation for the acoustic power spectrum due to cascade–turbulence interaction. *Journal of the Acoustical Society of America* 119 (2006) 108–122]. The MAP has been expressed as the sum of cut-on acoustic modes, whose modal power is the product of three terms: a term that specifies the wavenumber distribution of mean square velocity, a sound power factor that specifies the efficiency of radiation, and an acoustic blade response function. The effect of these terms on the MAP is discussed in detail in this paper. The acoustic blade response functions are found to determine the modal lines of minimum sound power in mode-frequency maps of the MAP. The upstream sound power factor is less than the downstream power factor, which is generally large, especially away from the cut-off frequency. Both power factors are small for modes close to cut-off. Modes close to cut-off, therefore, do not contribute significantly to the radiated acoustic power in the downstream direction, even though the modal pressure amplitude for these modes is high since they are excited close to resonance. For an isotropic turbulent gust, the mean square velocity wave number spectrum reduces only the magnitude of the MAP without altering the distribution of power in the frequency-mode map.

1. Introduction

With the reduction of jet noise and fan tone noise due to the introduction of higher bypass-ratio engines and lower-speed fans, fan broadband noise is now one of the major noise sources on an engine. This paper deals with the modal acoustic power (MAP) of broadband noise due to the interaction between isotropic homogeneous turbulence and a cascade of flat-plate airfoils. This problem is relevant to broadband noise generation in an aircraft engine due to the interaction of the turbulent rotor wakes with the stator vanes. This broadband-noise mechanism is now widely regarded as the dominant source of fan broadband noise.

*Corresponding author. Tel.: +82 51 510 3205; fax: +82 51 514 7640.
E-mail address: ccheong@pusan.ac.kr (C. Cheong).

0022-460X/$ - see front matter © 2009 Elsevier Ltd. All rights reserved.
doi:10.1016/j.jsv.2009.01.059

Nomenclature

a	sound speed
B	the number of airfoils in a cascade
c	airfoil chord length
k_i	wavenumber of ingested turbulence gust in Cartesian coordinate system
K_1	ω/W
l	acoustic mode number in the gap-wise direction
m	vortical mode number in the gap-wise direction
M	Mach number of mean-flow
M_1	Mach number in the axial direction, $M\cos\theta$
M_2	Mach number in the gap-wise direction, $M\sin\theta$
p	pressure perturbation
r	scattering index for a cascade of airfoils
R	cascade response function
s	blade spacing
t	time
u_i	velocity perturbation in x_i-direction
U_i	mean velocity in x_i-direction
w	upwash velocity perturbation
W	mean-flow speed, $\sqrt{U_1^2+U_2^2}$
x_i	Cartesian duct coordinate system, Fig. 1
y_i	Cartesian cascade-fixed coordinate system, Fig. 1
α	wavenumber of the generated disturbance in the axial-direction
β	wavenumber of the generated disturbance in the gap-wise direction
Γ	vortex strength
Δ	cut-on parameter
θ	stagger angle, $\tan^{-1}(U_2/U_1)$
Θ	cut-on ratio
λ	reduced frequency $\omega c/W$
ρ	density perturbation
σ	interblade phase angle
Φ_{ww}	turbulence spectrum
ω	angular frequency
PSD	power spectral density

One of the first attempts at predicting the broadband noise due to the interaction between an airfoil and a turbulence gust was by Amiet [1] who has developed a theory for broadband noise of a two-dimensional isolated airfoil in a turbulence stream. However, for an aero-engine fan, the number of blades is generally very high, such that acoustic interaction between the blades cannot be neglected. This leads us to consider the response of a blade row, or cascade, instead of isolated airfoils. The acoustic radiation from a uniformly spaced cascade of blades due to an impinging harmonic gust has been addressed using a number of different approaches. Kaji and Okazaki [2,3] have considered sound propagation upstream through a blade row by solving for the distribution of dipole source strength on the blade surfaces. Smith [4] has developed a numerical method for solving the unsteady flow through an infinite, two-dimensional cascade of flat plates at zero angle of attack. Further details are presented in Whitehead [5]. Mani and Hovray [6] have solved this problem using an approximate solution based on the Wiener Hopf method. Koch [7] has extended the method of Mani and Hovray to blades with finite chord. More recently, Peake [8] has extended Koch's analysis to determine the unsteady loading on the blades. Peake has also developed analytical tools to enable the rapid computation of the function required for the Wiener Hopf solution [9,10]. Glegg [11] has extended the method to a three-dimensional rectilinear cascade of blades, which allows the effect of blade sweep and of oblique gusts to be predicted.

The broadband noise radiated by a uniformly spaced cascade of blades due to an impinging turbulent gust may be predicted by Fourier synthesis of the response due to a single harmonic vortical gust. Hanson and Horan [12] have investigated this problem by extending the analytical model of Glegg [11]. Hanson [13] has used this model to investigate the effects of lean and sweep on broadband noise generation. Recent work of Cheong et al. [14] has extended the 2D solution of Smith [3] and Whitehead [4] to investigate the sound power radiated by a cascade of flat-plate airfoils interacting with two-dimensional homogeneous, isotropic turbulence. They found that the acoustic power spectrum may be conveniently split into two distinct frequency regions of low frequency and high frequency, separated by a critical frequency. Above this frequency, the blades were found to radiate incoherently and the acoustic power shown to be approximately proportional to the number of blades. Based on this finding, they derived an approximate formulation for the sound power

spectrum that is valid above the critical frequency and which is in excellent agreement with the exact expression for the broadband sound power spectrum.

Nose control in an aero-engine duct is generally based on the information about the modal distribution of the sound field in the engine duct [16]. This modal content will be largely determined by the distribution of cascade modes: for example, from the relative distribution of sound power in the co-rotating and contra-rotating modes. An understanding of the factors which influence this mode distribution is therefore essential. In the present study, the MAP generated by a cascade of flat-plate airfoils interacting with homogeneous, isotropic turbulence is investigated in detail. Emphasis is given to the characterization of the acoustic field through the breakdown into its MAP components. The basic formulation for the acoustic power upstream and downstream is based on the analytical theory of Smith [3] and its generalization due to Cheong et al. [14]. The MAP has been expressed as the sum of cut-on acoustic modes, whose modal power is the product of three terms: a term that specifies the wavenumber distribution of mean square velocity, a sound power factor that specifies the efficiency of radiation, and an acoustic blade response function. Through the analysis of each factor separately, their relative contributions to the MAP is assessed.

In Section 2, the method of Smith [3] and the extension to broadband noise of Cheong et al. [14] are briefly described. In Section 3, the formulation of MAP is decomposed into sub-components, which are analyzed independently. Finally, MAP distributions upstream and downstream are characterized in association with these factors.

2. Basic formulation for acoustic power spectrum

2.1. Brief review of the formulation of the acoustic power spectrum

The cascade geometry and coordinate system investigated in this paper is shown in Fig. 1. A two-dimensional cascade of flat-plate airfoils with stagger angle θ is assumed to be located in a two-dimensional uniform flow moving in the direction parallel to the chord, i.e., with zero angle of incidence. Homogeneous, isotropic turbulence is assumed to be convected with the mean flow W as a "frozen gust pattern". In Fig. 1, (x_1, x_2) is the unwrapped duct coordinate system, and (y_1, y_2) is the cascade-fixed coordinate system. Following Smith [3], nontrivial, single-frequency solutions of the governing linearized Euler equations of the form

$$\begin{pmatrix} u_1 \\ u_2 \\ p \end{pmatrix} = \begin{pmatrix} \bar{u}_1 \\ \bar{u}_2 \\ \bar{p} \end{pmatrix} e^{i(\omega t+\alpha x_1+\beta x_2)}, \tag{1}$$

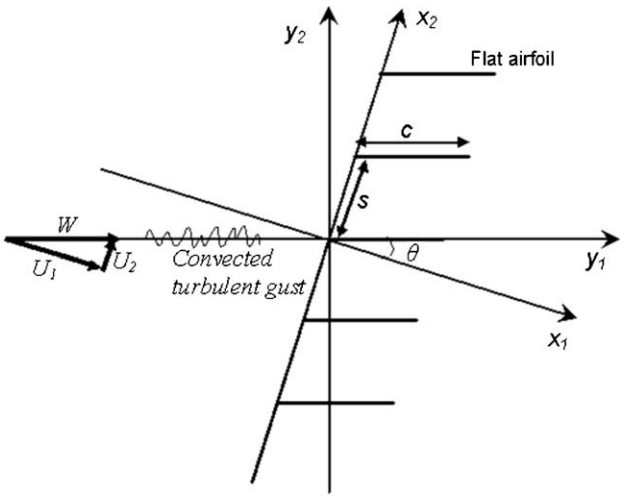

Fig. 1. The cascade geometry and its coordinate systems with the convected turbulent gust.

are obtained for

$$(\omega + U_1\alpha + U_2\beta)^2 - a^2(\alpha^2 + \beta^2) = 0, \tag{2}$$

or

$$(\omega + U_1\alpha + U_2\beta) = 0, \tag{3}$$

where $\bar{u}$ and $\bar{p}$ are complex amplitudes, and α and β are the wavenumbers of the perturbation quantities in the axial and gap-wise directions, respectively, and U_j is the mean velocity in the x_j-direction, u_i is the unsteady velocity perturbation in the x_i-direction, ρ_0 is the mean density, and p is the (acoustic) pressure. The dispersion relations of Eqs. (2) and (3) relate solely to acoustic waves and to vorticity waves, respectively. A single wavenumber component (k_1, k_2) of impinging turbulence has a phase angle σ between adjacent blades separated by a gap s given by

$$\sigma = (k_1 \sin\theta + k_2 \cos\theta)s. \tag{4}$$

The phase angle $\beta_r s$ between adjacent blades of the rth acoustic wave generated from the cascade due to a single wavenumber component of vorticity (k_1, k_2) is of the form $\beta_r s = \sigma - 2\pi r$ $(r = -\infty, \ldots, -1, 0, 1, \ldots, \infty)$. The acoustic circumferential wave number β_r of the rth acoustic wave is therefore given by

$$\beta_r = \frac{(k_1 \sin\theta + k_2 \cos\theta)s - 2\pi r}{s}. \tag{5}$$

Eq. (2) is a quadratic equation of the axial wavenumber α, whose solution can be expressed in terms of β_r and ω as follows:

$$\alpha_r^{\pm} = \frac{M_1(\omega/a + M_2\beta_r) \pm \sqrt{(\omega/a + M_2\beta_r)^2 - (1 - M_1^2)\beta_r^2}}{1 - M_1^2}. \tag{6}$$

The two solutions for α_r correspond to upstream going $(+)$ and downstream going $(-)$ acoustic waves. Note that β_r takes an infinite number of values, corresponding to an infinite number of cascade modes. However, Eq. (6) indicates that only a finite number of these modes can propagate unattenuated. The amplitude of the cascade modes due to a harmonic gust can be obtained by following the procedure presented by Smith [3]. For a harmonic gust of the form

$$w(y_1, y_2, t) = w_0 e^{i[k_1(y_1 - Wt) + k_2 y_2]}, \tag{7}$$

the acoustic pressure upstream and downstream of the cascade $(+,-)$ is of the form

$$p^{\pm}(x_1, x_2, t) = \rho_0 W w_0 \sum_{r=-\infty}^{\infty} R_r^{\pm} e^{i(k_1 Wt + \alpha_r x_1 + \beta_r x_2)}, \tag{8}$$

where $R_r^{\pm}$ is the cascade response function, which specifies the nondimensional modal pressure amplitude and is completely defined by the parameters of s/c, θ, M, λ and σ, where λ is the reduced frequency $\omega c/W$.

The analysis of sound radiation due to an incident sinusoidal vortical gust can be extended to broadband turbulent velocity distributions via Fourier transformation. It is assumed here that the turbulence can be regarded as a "frozen gust pattern" convecting with the free stream velocity W. This is a reasonable assumption because turbulence velocities are generally much smaller than convection velocities and hence change only slightly as they are convected past any airfoil in the cascade. Eq. (8) can be generalized to give the acoustic pressure radiated from a cascade subject to the impinging turbulent gust, in the form

$$p^{\pm}(x_1, x_2, t) = \rho_0 W \int_{-\infty}^{\infty}\int_{-\infty}^{\infty} \hat{\hat{w}}(k_1, k_2) \sum_{r=-\infty}^{\infty} R_r^{\pm}(k_1, k_2) e^{i(k_1 Wt + \alpha_r^{\pm} x_1 + \beta_r x_2)}\, dk_1\, dk_2, \tag{9}$$

where $\hat{\hat{w}}(k_1, k_2)$ is the two-dimensional wavenumber spectrum of the turbulence velocity in the direction normal to the blade. By following the procedure described by Cheong et al. [14], the acoustic spectrum of

sound power per unit span can be expressed in the form

$$\mathscr{P}^{\pm}(\omega) = \frac{2\pi\rho_0 M}{\cos\theta} \sum_{l=-\infty}^{\infty} Q_l^{\pm}(K_1) \sum_{r=-\infty}^{\infty} \Phi_{ww}(K_1, k_{2,l+Br}), \tag{10}$$

where $Q_l^{\pm}$ is a nondimensional modal power response function given by

$$Q_l^{\pm}(K_1) = |R_l^{\pm}(K_1, k_{2,\mathrm{mod}(l,B)})|^2 \frac{\omega\,\mathrm{Re}\{-a\alpha_l^{\pm} + M_1(\omega + U_1\alpha_l^{\pm} + U_2\beta_l)\}}{|\omega + U_1\alpha_l^{\pm} + U_2\beta_l|^2} \tag{11}$$

and the acoustic wavenumber in the x_2-direction must satisfy the periodicity condition

$$\beta_l = \frac{2\pi}{Bs} l, \tag{12}$$

where l is an arbitrary integer and denotes the order of the acoustic mode in the x_2-direction (which coincides with the circumferential direction in the duct coordinate system).The function, mod(l, B), denotes the remainder when the first argument is divided by the second argument. If we consider only the cut-on modal components in Eq. (10), the infinite summation over l in Eq. (10) becomes finite at a given frequency. In a subsonic flow, $W<a$, propagating modes correspond to real values of $\alpha_r^{\pm}$ in Eq. (6), which depends upon the sign of the expression under the square root of Eq. (6), which may be written in the form

$$\Delta_l^2 = (k + M_2\beta_l)^2[1 - \Theta_l^2], \tag{13}$$

where Θ_l is a nondimensional cut-on parameter defined by

$$\Theta_l = \frac{\sqrt{1 - M_1^2}\beta_l}{k + M_2\beta_l}. \tag{14}$$

Eq. (13) defines the cut-on condition of the cascade modes. If $\Delta_l^2 > 0$, or $\Theta_l^2 < 1$, the acoustic axial wavenumber is purely real and the acoustic waves propagate unattenuated. We denote $L_{\max}$ and $L_{\min}$ as the maximum and minimum integers of the acoustic mode number l satisfying the inequality of $\Delta_l^2 > 0$, or $\Theta_l^2 < 1$. These correspond to acoustic modes traveling in the direction of the swirl velocity U_2, and against it, respectively. Eq. (10) can now be written as

$$\mathscr{P}^{\pm}(\omega) = \frac{2\pi\rho_0 M}{\cos\theta} \sum_{l=L_{\min}}^{L_{\max}} Q_l^{\pm}(K_1) \sum_{r=-\infty}^{\infty} \Phi_{ww}(K_1, k_{2,l+Br}), \tag{15}$$

where the range of the scattering index r is chosen to ensure convergence of the solution.

For simplicity we assume that the turbulence impinging on the cascade is homogeneous and isotropic. A suitable model for wavenumber PSD (power spectral density), that is consistent with these requirements, is the Liepmann spectrum $\Phi_{ww}(k_1, k_2, k_3)$ of the form

$$\Phi_{ww}(k_1, k_2, k_3) = \frac{2\overline{w^2}\Lambda^3}{\pi^2} \frac{\Lambda^2(k_1^2 + k_2^2)}{[1 + \Lambda^2(k_1^2 + k_2^2 + k_3^2)]^3}, \tag{16}$$

where $\overline{w^2}$ is the mean square value of turbulence velocity in the direction normal to the chord and Λ is the turbulence integral length-scale. Integrating over k_3 gives the two-dimensional spectrum required in Eq. (15) of the form

$$\Phi_{ww}(k_1, k_2) = \frac{\overline{w^2}\Lambda^2}{4\pi} \frac{[1 + \Lambda^2(4k_1^2 + k_2^2)]}{[1 + \Lambda^2(k_1^2 + k_2^2)]^{5/2}}. \tag{17}$$

2.2. Comparison with measured data

A comparison between the sound power spectra predicted using Eq. (15) and the experimental data obtained from a model test in a wind tunnel at NASA-Lewis [12] was shown in Fig. 9 in Ref. [14], which had been computed by the author using the same formulation. The computation were performed for $B=45$, $s/c=0.8$, $\theta=30^\circ$ at $M=0.5$. The incident turbulence flow is assumed to be homogeneous and isotropic and modeled using Eq. (17) with $\overline{w^2}/W^2=4\times10^{-4}$ and $\Lambda/c=0.2$. The turbulence length-scale and intensity were determined by trial and error to provide a good fit to the measured data. The measured noise below 300 Hz was reported to be due to sources other than the fan. Although the prediction was carried out using two-dimensional theory and the turbulence assumed to have the idealized characteristics described above, predictions from the theoretical model were found to be in acceptable agreement with the experimental data.

The broadband noise in an aircraft engine, which the model described above is believed to a good model for, is generated mainly through the interaction between the turbulent rotor wakes and the stator vanes. In this respect, the turbulence velocity field may be inhomogeneous, which may be related to blade-to-blade variations and variations across the span of the vanes. However, Hanson and Horan [12] have derived the expression for the acoustic power spectrum including turbulence inhomogeneity, and show that this generalization simply requires the use of an average spectrum for homogeneous turbulence. This finding legitimizes the use of this analysis for inhomogeneous flows and suggests that the adjusted values of the turbulent length scale and intensity in homogeneous turbulence spectrum may be considered to represent the averaged value of those in the inhomogeneous turbulence spectrum.

3. Decomposition of MAP

As shown in the previous section, the total acoustic power spectrum can be represented as the superposition of the acoustic power spectra of all propagating acoustic modes l, each of which is generated by an infinite number of vortical modes satisfying the scattering rule, $m=l+Br$. The acoustic power of the lth mode is therefore given by

$$\mathscr{P}_l^{\pm}(\omega)=\frac{2\pi\rho_0 M}{\cos\theta}Q_l^{\pm}(\omega)\left(\sum_{r=-\infty}^{\infty}\Phi_{ww}(K_1,k_{2,l+Br})\right). \tag{18}$$

Fig. 2a and b shows the mode-frequency map (power versus l and λ) of the predicted upstream and downstream acoustic power spectra shown in Fig. 9 in Ref. [14]. Modes contributing to the acoustic power are found to be located between the two cut-off lines, which can be obtained by solving the inequality equation, $\Theta_l^2<1$, from Eq. (14)

$$\lambda\frac{Bs}{2\pi c}\frac{M_2-(1-M_1^2)^{1/2}}{1-M^2}\leqslant l\leqslant\lambda\frac{Bs}{2\pi c}\frac{M_2+(1-M_1^2)^{1/2}}{1-M^2}. \tag{19}$$

Although in Fig. 9 in Ref. [14] the upstream and downstream acoustic power spectra are similar in shape, their modal distributions differ significantly, as shown in Fig. 2. However, common and different characteristics for the MAP distributions of upstream and downstream propagating waves can be identified. The common characteristics are that the modal power distribution diminishes as the frequency increases and that modes near the cut-off lines are generally larger than the others. Another interesting common feature of these figures is that there exists a line of minimum MAP, which we delineate by the dash-dot lines in Fig. 2. An expression for the location of these power minima will be derived below. The different characteristics is that, in the upstream radiated acoustic field, the modes near the cut-off lines dominate the power spectrum while, in the downstream direction, the modes away from the cut-lines make a larger contribution to the power spectrum.

Fig. 3a–d shows the MAP of Fig. 2 in terms of the acoustic mode order l at four representative frequencies.

In an attempt to explain the characteristics of MAP distributions observed in Figs. 2 and 3, the formulation for the MAP spectrum, Eq. (18), is decomposed into two main terms. The first term corresponds to the modal

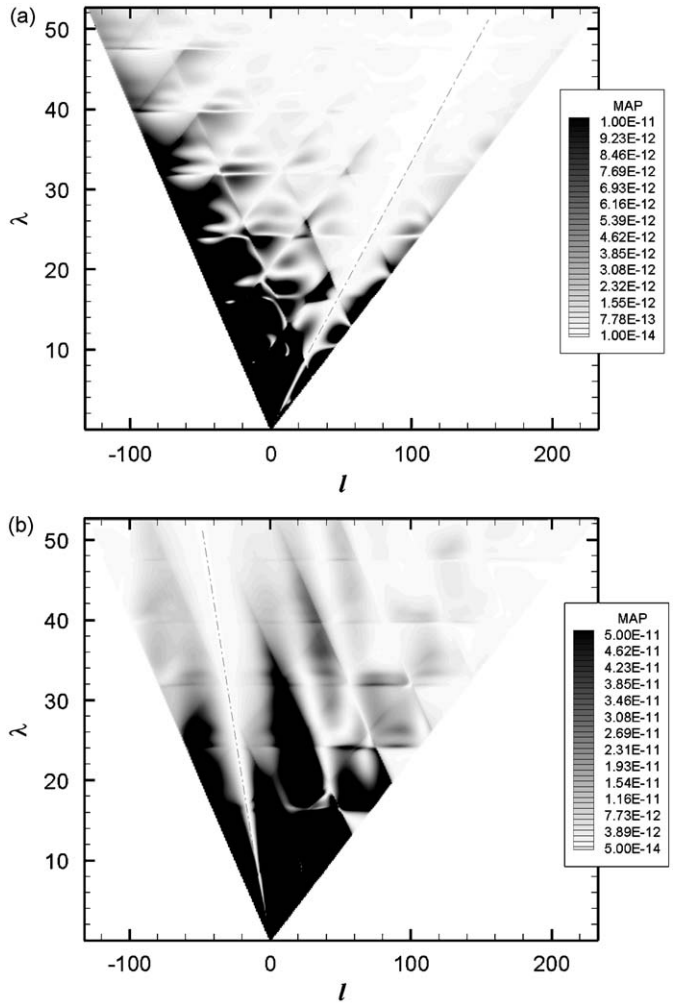

Fig. 2. The predicted nondimensional modal acoustic power (MAP) in the mode-frequency map for the model of $B = 45$, $s/c = 0.8$, $\theta = 30^\circ$ at $M = 0.5$ and the turbulence spectrum with $\overline{w^2}/W^2 = 4 \times 10^{-4}$ and $\Lambda/c = 0.2$: (a) upstream and (b) downstream.

power response function $Q_l^{\pm}$ defined by Eq. (11):

$$Q_l^{\pm} = |R_l^{\pm}|^2 \zeta_l^{\pm}, \tag{20}$$

where $\zeta_l^{\pm}$ is the nondimensional acoustic power factor defined by

$$\zeta_l^{\pm} = \frac{\omega \,\mathrm{Re}(-a\alpha_l^{\pm *} + M_1(\omega + U_1\alpha_l^{\pm *} + U_2\beta_l))}{|\omega + U_1\alpha_l^{\pm} + U_2\beta_l|^2}. \tag{21}$$

The second term is in the form of an infinite sum of the turbulence spectra scattered into the mode l.

Fig. 4 depicts the MAP together with the MAP response function $Q_l^{\pm}$ and the turbulence series plotted against the acoustic mode order l. These result are obtained using the same conditions as in the previous reference case at the reduced frequencies, $\lambda = 21.11$ and 42.16. This figure shows that the MAP distribution is principally determined by the MAP response function since the variation of the turbulence series with l stays almost constant. Similar results are obtained for all other frequencies and configurations.

Having established that the modal power distribution is predominantly controlled by the cascade response function and not the distribution of vortical modes we now investigate the behavior of the MAP response function $Q_l^{\pm}$ in greater detail. Eq. (20) shows that the $Q_l^{\pm}$ can be expressed in the form $Q_l^{\pm} = |R_l^{\pm}|^2 \zeta_l^{\pm}$. In the following, both terms will be studied to determine their contribution to the MAP response function.

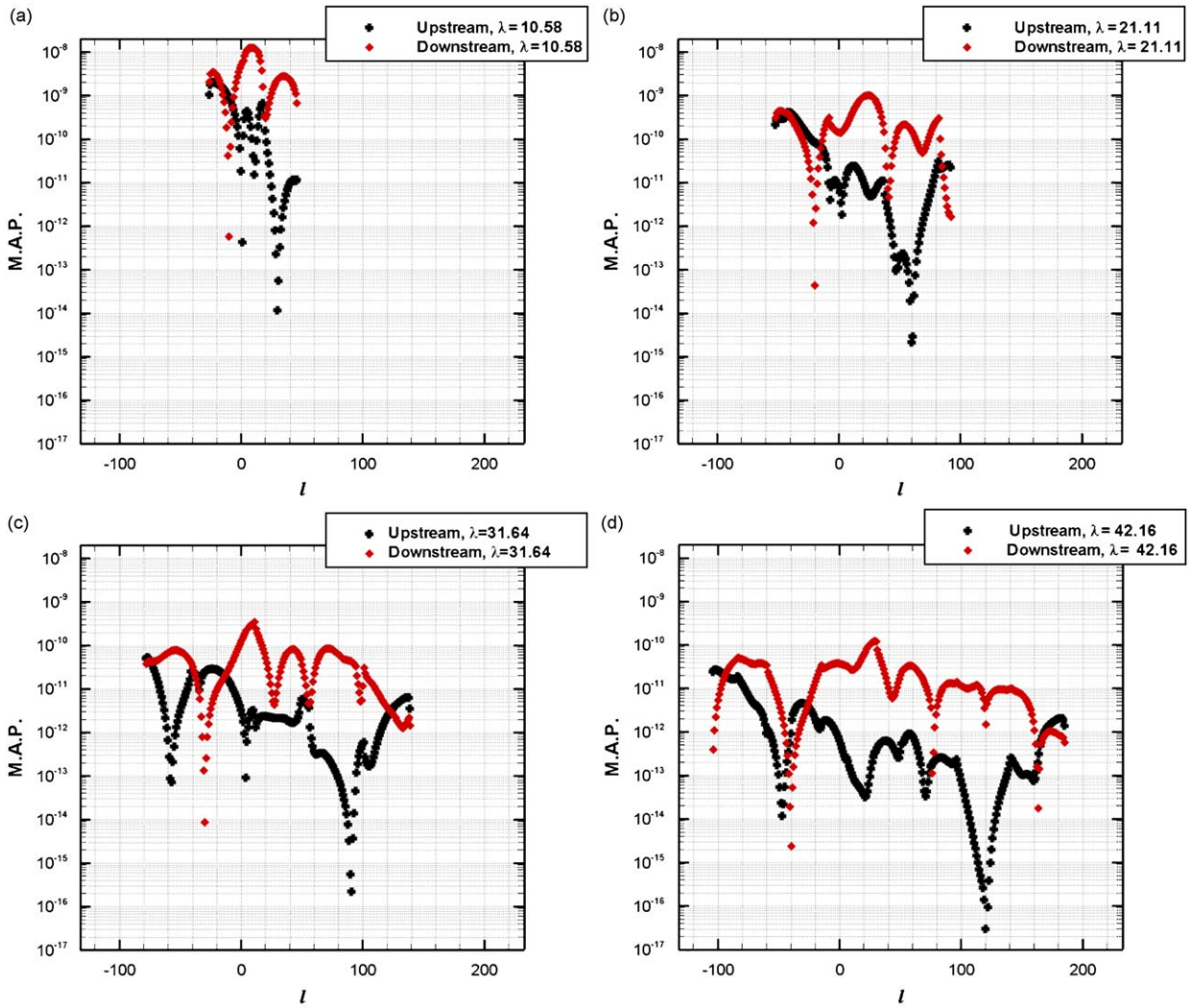

Fig. 3. Predicted nondimensional modal acoustic power (MAP) versus acoustic mode number l at: (a) $\lambda = 10.58$, (b) $\lambda = 21.11$, (c) $\lambda = 31.64$ and (d) $\lambda = 42.16$. ■: Upstream and ◆: downstream.

3.1. Modal acoustic pressure response function

The modal acoustic pressure response function $R_l^{\pm}$ is obtained from an approximate solution of the integral equation by the use of the collocation technique [3,4]. The modal acoustic pressure response function defined in Eq. (8) can be expressed in the matrix form [3,4];

$$R_l^{\pm} = (X_l^{\pm})_j K_{ji}^{-1} W_i, \tag{22}$$

where $K_{ji}^{-1} W_i$ denotes the approximate solution of the bound vortex distribution at the j-th discretized point on the blades. The vector $X_l^{\pm}$ relating the vortex distribution to the modal acoustic pressure can be also decomposed into two terms as follows:

$$X_l^{\pm} = |V_l^{\pm}| x_l^{\pm}, \tag{23}$$

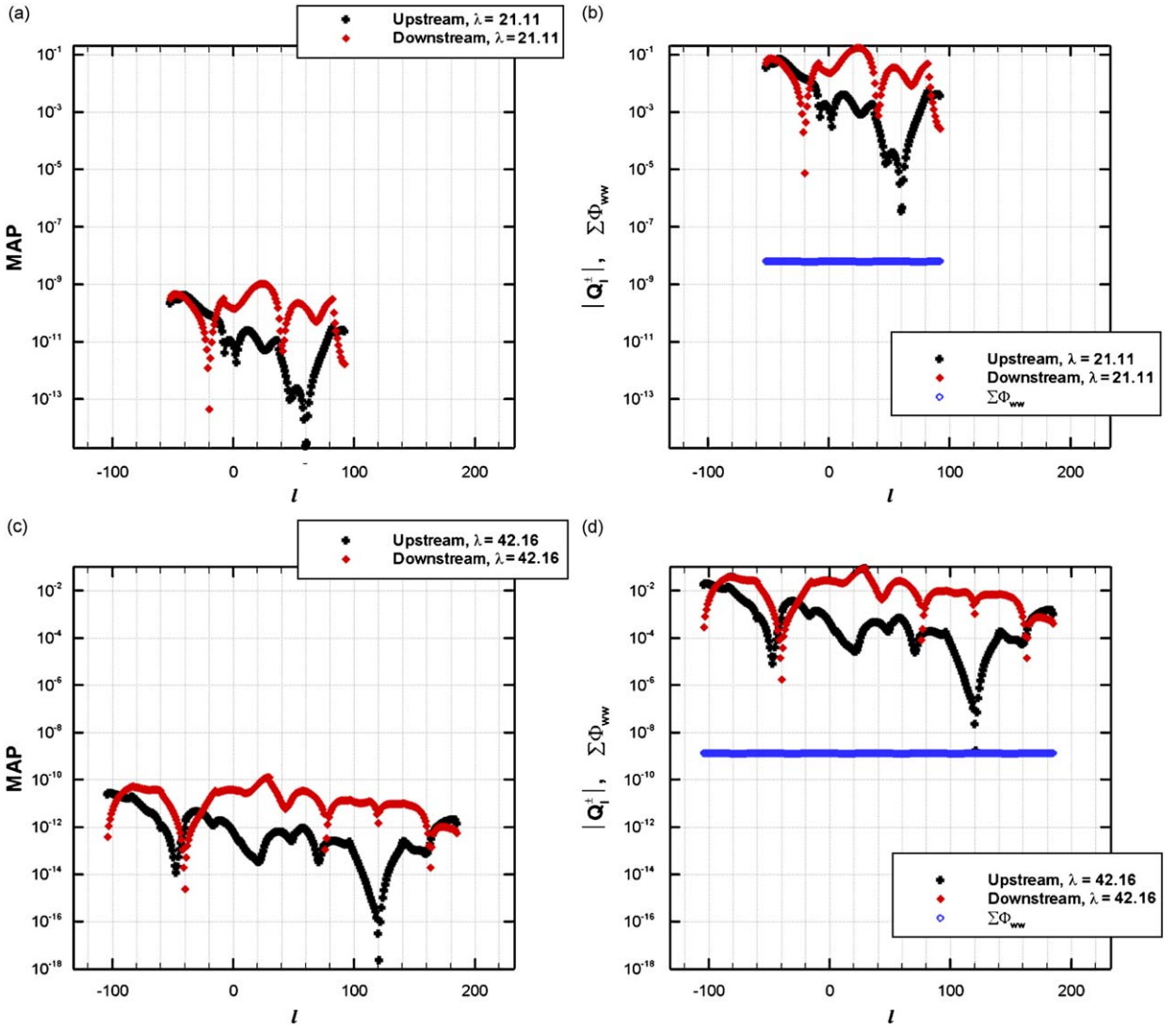

Fig. 4. The nondimensional modal acoustic power (MAP), $|Q_l^{\pm}|$ and $\Sigma\Phi_{ww}$ versus acoustic mode order l at: (a) $\lambda = 21.11$, (b) $\lambda = 21.11$, (c) $\lambda = 42.16$ and (d) $\lambda = 42.16$. ■: Upstream; ◆: downstream; and ◦: $\Sigma\Phi_{ww}$.

where the real factor $V_l^{\pm}$ is defined by

$$V_l^{\pm} = -\frac{(v')^{\pm}}{(s/c)}\frac{(\lambda + \hat{\alpha}_l^{\pm}\cos\theta + \hat{\beta}_l \sin\theta)}{\hat{\beta}} \tag{24}$$

and the vector $x_l^{\pm}$ is the phase vector of $X_l^{\pm}$, with the j-th element defined by

$$(x_l^{\pm})_j = \exp\left[-\mathrm{i}(\hat{\alpha}^{\pm}\cos\theta + \hat{\beta}\sin\theta)\left(1 - \cos\frac{\pi j}{N}\right) + \mathrm{i}\phi\right], \tag{25}$$

where the phase φ is introduced to give the correct sign to the term $V_l^{\pm}$. The phase is then equal to 0 if for the lth acoustic mode the value of $V_l^{\pm}$ is positive and π, if this term is negative. Eq. (22) can therefore be written as

$$R_l^{\pm} = |V_l^{\pm}|(x_l^{\pm})_j K_{ji}^{-1} W_i. \tag{26}$$

3.1.1. Analysis of $V_l^{\pm}$

Use of Eq. (6) for the axial acoustic wavenumber allows the second term in the right-hand side of Eq. (24) for $V_l^{\pm}$ to be expressed as a function of the circumferential wavenumber β_l and the cut-on parameter Δ_l:

$$\frac{(\lambda+\hat{\alpha}_l^{\pm}\cos\theta+\hat{\beta}_l\sin\theta)}{\hat{\beta}}=\frac{K_1+\beta_l\sin\theta\pm\Delta_l\cos\theta}{\beta_l(1-M_1^2)}. \tag{27}$$

The first term in the right-hand side of Eq. (24), the reduced velocity, can also be expressed in terms of β_l and Δ_l:

$$v'^{\pm}=\frac{\beta_l}{2\Delta_l(\beta_l^2+\Delta_l^2)}[kM_1\beta_l\mp\Delta_l(M^2\beta_l+kM_2)]. \tag{28}$$

The product of Eqs. (27) and (28) allows the modulus of $V_l^{\pm}$ to be expressed as the sum of two terms. The first is common to both upstream and downstream propagating waves, the second term differs in the two propagation directions. The term $V_l^{\pm}$ can then be expressed by Jurdic [15] in the form

$$V_l^{\pm}=\frac{c}{s}\frac{1}{2\Delta_l(\beta_l^2+\Delta_l^2)(1-M_1^2)}(Y_1\pm\Delta_l Y_2), \tag{29}$$

where after simplifications:

$$Y_1=(\Delta_l^2+\beta_l^2)[M_2(k+M_2\beta_l)-(1-M_1^2)\beta_l]\cos\theta, \tag{30}$$

$$Y_2=\frac{M_2}{M}(\Delta_l^2+\beta_l^2). \tag{31}$$

By introducing the cut-on ratio Θ defined in Eq. (14) into Eq. (29), $V_l^{\pm}$ can be expressed in terms of Θ,

$$V_l^{\pm}(\Theta,M,\theta)=\frac{c}{s}\left[\frac{\cos\theta}{2\sqrt{1-M_1^2}\sqrt{1-\Theta_l^2}}\left(\frac{M_2}{\sqrt{1-M_1^2}}-\Theta\right)\pm\frac{\sin\theta}{2\beta_1^2}\right]. \tag{32}$$

Fig. 5a and b is a plot of $|V_l^{\pm}|$ at different frequencies for a reference case, plotted against l and Θ, respectively. Fig. 5 demonstrates that $|V_l^{\pm}|$ has a minimum value for specific discrete values of l or Θ_l. An estimate for when this occurs can be obtained by considering the expression of Eq. (32) for $|V_l^{\pm}|$ to be a continuous function. Defining Θ^+ and Θ^- as the values of cut-on ratio at which the values of $|V_l^{\pm}|=0$ for the upstream and downstream propagating waves, respectively, setting $V_l^{\pm}$ of Eq. (32) to zero leads to

$$\Theta^+=\frac{M_2\sqrt{1-M_1^2}}{M-M_1^2} \tag{33}$$

for upstream waves while for downstream propagating waves

$$\Theta^-=-\frac{M_2\sqrt{1-M_1^2}}{M+M_1^2}. \tag{34}$$

This condition corresponds to a mode number l for upstream radiation as

$$l^+=\frac{Bs}{2\pi c}\frac{\lambda\sin\theta}{1-M} \tag{35}$$

and for downstream radiation as

$$l^-=-\frac{Bs}{2\pi c}\frac{\lambda\sin\theta}{1+M}. \tag{36}$$

as shown in Fig. 5.

Eqs. (35) and (36) indicate that the modes containing minimum sound power may be represented by the lines in the mode-frequency map shown previously in Fig. 2. It can also be found in Eqs. (35) and (36) that the

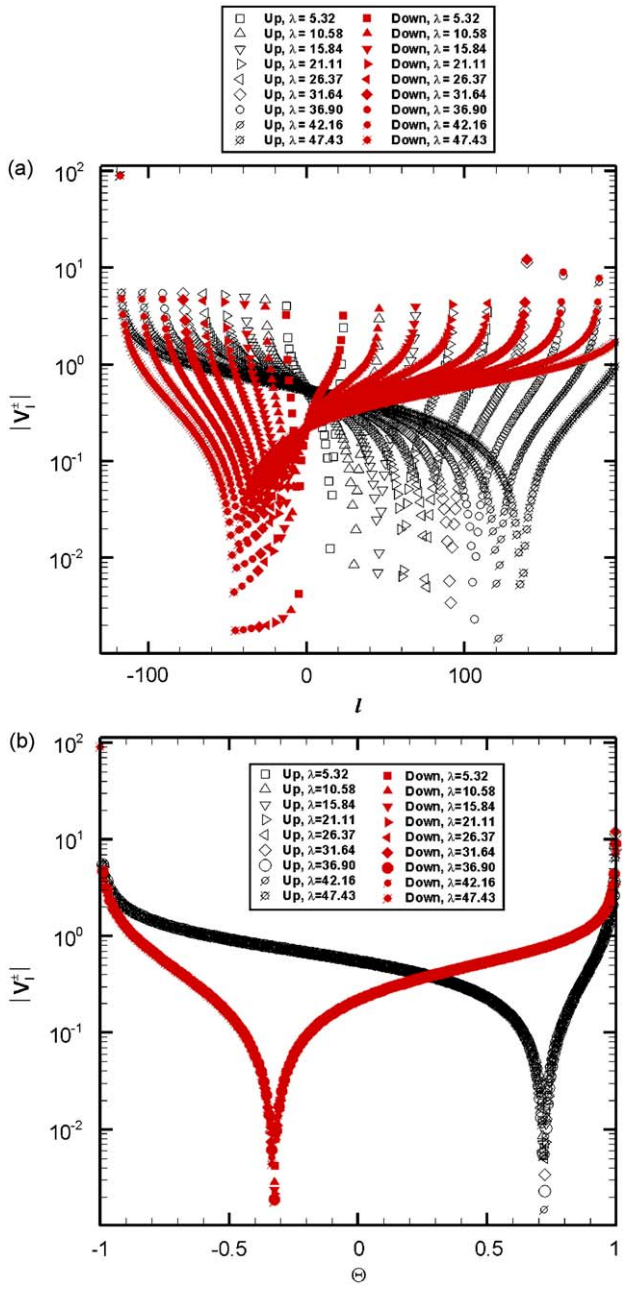

Fig. 5. The modulus of $X_l^{\pm}$, $|V_l^{\pm}|$ versus: (a) acoustic mode order l and (b) the cut-on parameter Θ.

slope of the lines is a function of stagger angle, Mach number, solidity and blade number: $2\pi c(1-M)/\sin(\theta)Bs$ for upstream and $-2\pi c(1+M)/\sin(\theta)Bs$ for downstream, respectively. Comparing Eqs. (35) and (36) with Eq. (19), these minimum lines are always located between the cut-off lines for subsonic flow. This suggest that there will always be lines of minimum MAP in the mode-frequency map of acoustic power, similar to the dash-dotted lines in Fig. 3. In addition, combining Eqs. (33) and (34) with (6), we can find that the ratio of wavenumber components of acoustic wave at $V_l^{\pm} = 0$ satisfies the relation:

$$\frac{\beta_l}{\alpha_l^{\pm}} = \mp \tan\,\theta. \tag{37}$$

This equation indicates that the scattered pressure associated with these zero-pressure modes propagates parallel to the chord for which the acoustic dipoles on the blade surface generate no power as explained by Glegg [11].

Fig. 5(b) show that $|V_l^{\pm}|$ is a unique function of cut-on ratio Θ_l, suggesting that the modulus of the transfer function $X_l^{\pm}$ between the vortex distribution and acoustic pressure are uniquely determined, independent of frequency. A specific frequency will determine the number of cut-on modes according to Eq. (19). The corresponding transfer function modulus between the vortex distribution and modal acoustic pressure is given by only a few discrete points of the curve as described above. The absolute value of the corresponding parameter Θ_l for the same mode at two different frequencies will then be larger for the lower frequency than for the higher one. Therefore, the magnitude of the transfer function $X_l^{\pm}$ will be higher at the lower frequency than at the higher frequency. This characteristic of $X_l^{\pm}$ leads to the modes in the lower frequency range contributing more to acoustic power than those in higher frequency range, which is described as one of the characteristics in the MAP distribution in Fig. 2.

3.1.2. *Analysis of modulus of* $(x_l^{\pm})_j K_{ji}^{-1} W_i$

The cascade modal function defined in Eq. (26) includes the term $(x_l^{\pm})_j K_{ji}^{-1} W_i$. In this section, the modulus of the product of the phase vector $(x_l^{\pm})_j$ and the bound vortex distribution along the blades defined by $K_{ji}^{-1} W_i$ is investigated. From Eq. (26), this term is equal to the ratio of $|R_l^{\pm}|/|V_l^{\pm}|$ which may be interpreted as the sum of the strengths of all the bound vortices occupying the location of the flat-airfoil cascades, multiplied by a relative phase angle between the l-th acoustic mode and the position of the vortex.

Fig. 6a–d shows the ratio $|R_l^{\pm}|/|V_l^{\pm}|$ plotted against l for a reference vane at different reduced frequencies. Comparing Fig. 6 with Fig. 3, we find that the modal distribution of the term $(x_l^{\pm})_j K_{ji}^{-1} W_i$ determines the detailed MAP distribution. The magnitudes of the upstream and downstream responses of the cascade are comparable for each of the cut-on mode and do not decrease significantly as the frequency increases. Note that the upstream propagating modes, in general, contribute less than for the downstream propagating modes.

3.2. *Modal power factor term*

An important factor in determining the sound power distribution of the acoustic modes in the uniform mean flow is the modal power factor $\zeta_l^{\pm}$. The modal power factor is defined by Eq. (21), and can be expressed in the form [15]:

$$\zeta_l^{\pm} = \mp \frac{kM_1^2 \,\mathrm{Re}(\Delta_l)}{(\alpha_l^{\pm} \mp \Delta_l)^2}. \tag{38}$$

Note that, when there is no mean flow, Eq. (38) reduces to $\zeta_l^{\pm} = -\mathrm{Re}(\alpha_l^{\pm})/k$. When the term Δ_l defined in Eq. (13) is real, the l-th acoustic wave contributes to the total acoustic power. However, when Δ_l is imaginary, i.e., the acoustic mode l is cut-off, the power factor becomes zero and the acoustic wave therefore does not contribute to the acoustic power. For the cut-on acoustic modes, introducing Eq. (6) for the axial wavenumber $\alpha_l^{\pm}$ into Eq. (38), the power factor term can be expressed in the form [15]:

$$\zeta_l^{\pm} = \mp(1 - M_1^2)\left(1 - \frac{M_2\Theta_l}{\sqrt{1 - M_1^2}}\right)\frac{\sqrt{1 - \Theta_l^2}}{\left[1 \pm M_1\sqrt{1 - \Theta_l^2}\right]^2}. \tag{39}$$

Using Eqs. (38) and (39), the power factor term is plotted in Fig. 7 for the reference case at different reduced frequencies. The upstream power factor is observed to be relatively flat apart for the modes close to cut-off, while the downstream power factor follows a more rounded-shape, increasing the magnitude of some modes more than others. Also the magnitude of the power factor of the downstream propagating waves is approximately an order of magnitude greater than that of the upstream going waves. This difference is the main reason for the difference in upstream and downstream acoustic power spectra observed in Fig. 3. Note that this difference increases as the flow Mach number onto the vanes increases. Fig. 7(b) shows that, similar

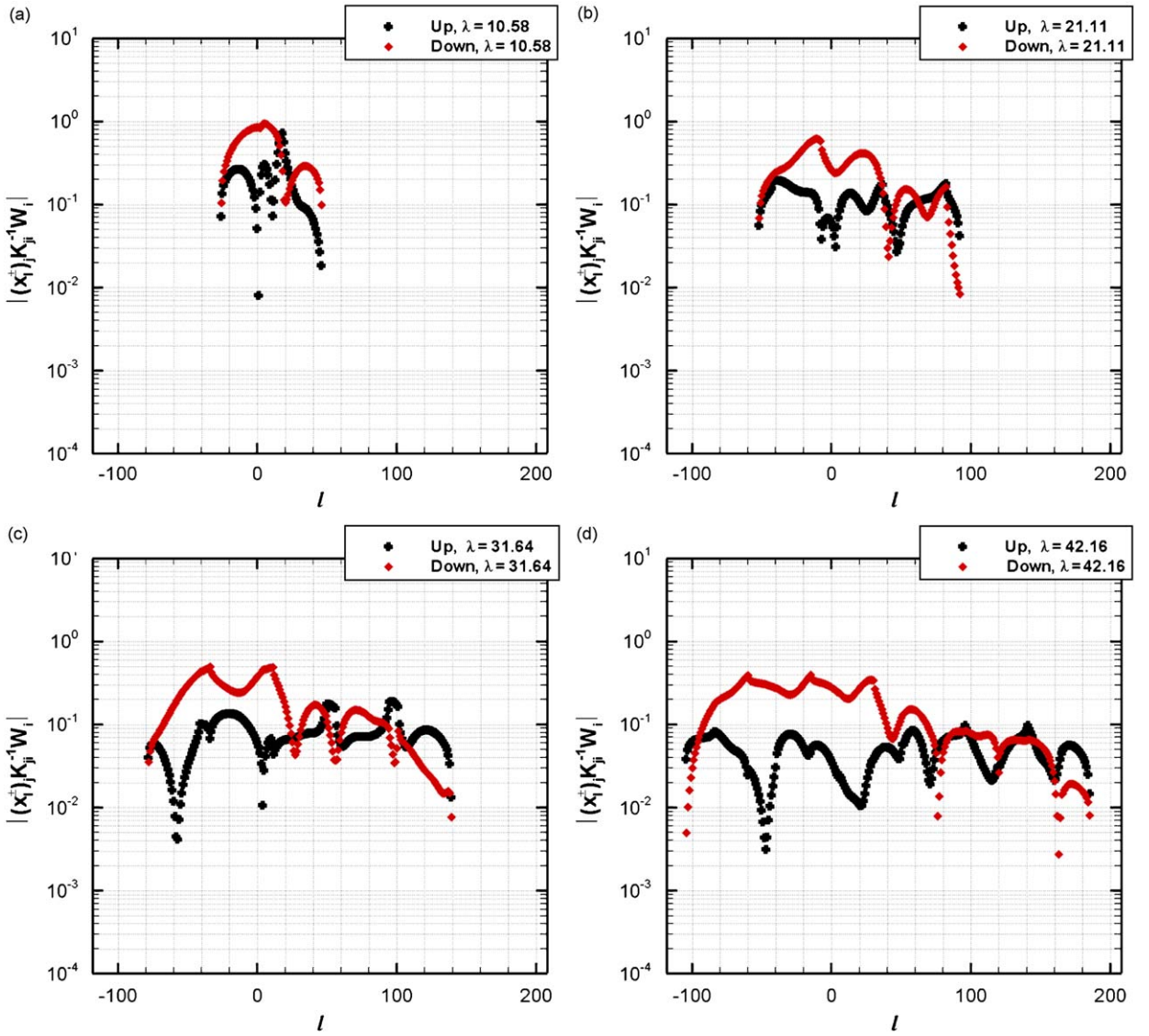

Fig. 6. $|(x_l^{\pm})_j K_{ji}^{-1} W_i|$ versus acoustic mode order l for the reference vane: (a) at $\lambda = 10.58$, (b) at $\lambda = 21.11$, (c) $\lambda = 31.64$ and (d) $\lambda = 42.16$. ■: Upstream and ◆: downstream.

to $|X_l^{\pm}|$, the power factor term $|\zeta_l^{\pm}|$ can be represented by a unique curve when expressed as a function as a function of Θ.

4. Response function of MAP

The upstream and downstream MAP response function $Q_l^{\pm}$ is plotted in Fig. 8 versus the acoustic mode order l together with its constituent components: $|(x_l^{\pm})_j K_{ji}^{-1} W_i|^2$, $|V_l^{\pm}|^2$ and the power factor $\zeta_l^{\pm}$. These figures clearly demonstrate the effects of each component on the MAP response function. The term $|(x_l^{\pm})_j K_{ji}^{-1} W_i|^2$ is observed to make the dominant contribution to the variation of $Q_l^{\pm}$ with l. The term $|V_l^{\pm}|^2$ characterizes the minimum values $Q_l^{\pm}$ near the mode numbers defined in Eqs. (35) and (36) and, at the same time, increases the magnitude of the modal power near modal cut-off. However, the power factor term $\zeta_l^{\pm}$ decreases the magnitude of modes near cut-off. For the modes near cut-off, therefore, the effect of the term $|V_l^{\pm}|^2$ and the power factor $\zeta^{\pm}$ very nearly cancel such that the combined effect is negligible. This means that, although

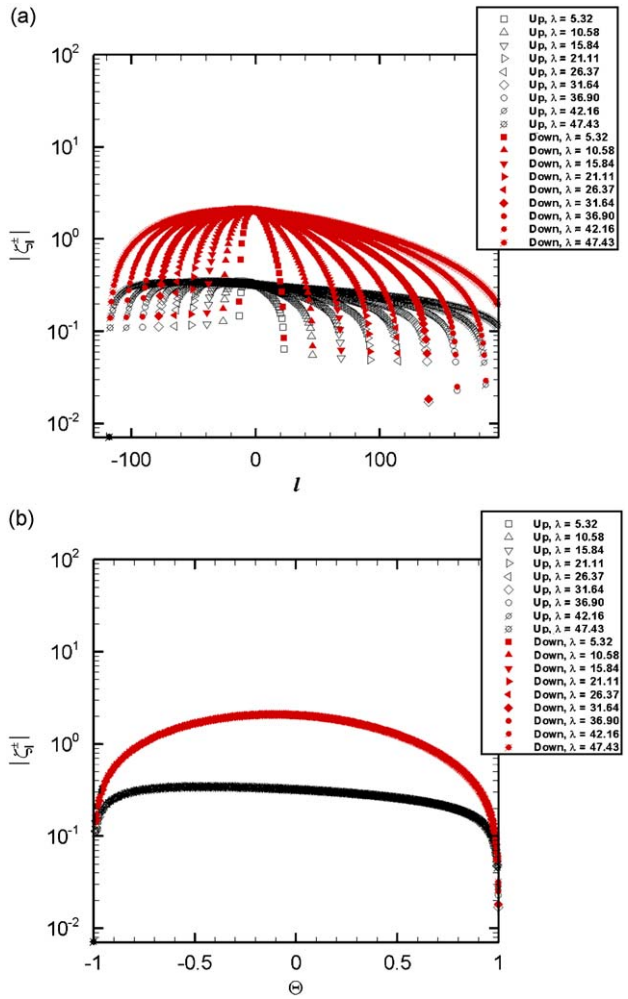

Fig. 7. The power factor, $|\zeta_l^{\pm}|$ versus: (a) acoustic mode order l and (b) the cut-on parameter Θ at different reduced frequency.

the magnitudes of modal acoustic pressure near cut-off are large, the MAP near cut-off makes a relatively small contribution to the total acoustic power. The power factor ζ^+ for the upstream direction is observed to stay almost constant, decreasing the magnitude of modes located in the center region away from two cut-off modes at a given frequency while, in the downstream direction, the power factor ζ^- tends to increase modes. This implies that, as previously observed in Figs. 2 and 3, the modes away from cut-off contribute highly to the radiated acoustic power in the downstream direction.

It is noted that the modal acoustic pressure response function, R, become infinite at the modal cut-off due to the factor $(1–\Theta^2)^{0.5}$ in the term, V, in Eq. (32) where the cut-on ratio $\Theta = 1$ at the cut-off. However, the origin of the factor $(1–\Theta^2)^{0.5}$ originates from the acoustic particle velocities in Eq. (23) in Ref. [4], which are derived from three conservation equations: the conservation of mass, the velocity jump in the y-direction being equal to the strength of the wave, and the conservation of vorticity. At $\Theta = 1$, the equation of continuity, Eq. (19) in Ref. [4], becomes insoluble. Therefore, the form of R is only valid in the ranges of $|\Theta| < 1$ and $|\Theta| > 1$. It seems to be more insightful to understand the behavior of R (or V) at $\Theta = 1$ in terms of the limiting value of R as Θ approaches 1, which shows that R takes a finite value at $\Theta = 1$. However, the power factor term, ζ, includes the factor $(1–\Theta^2)^{0.5}$ in the numerator as shown in Eq. (38). The multiplication of the acoustic pressure response function and the power factor leads to the magnitudes of modal power becoming zero at cut-off. The same dependence of the acoustic power, i.e., $(1–\Theta^2)^{0.5}$ at the cut-off, has been reported by Glegg [14] using the Wiener Hopf method.

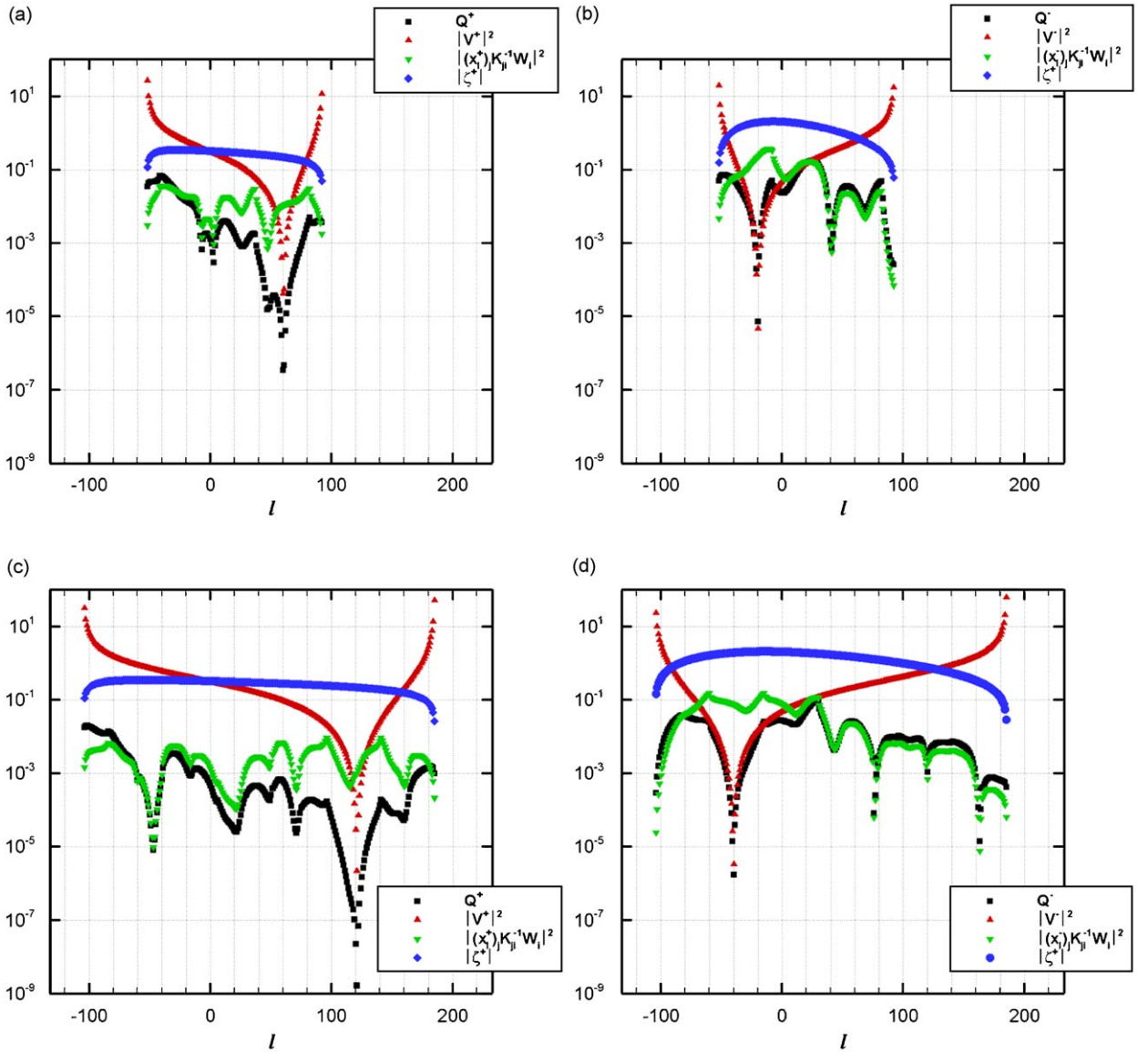

Fig. 8. Decomposition of modal acoustic power response function: (a) upstream at $\lambda = 21.11$, (b) downstream at $\lambda = 21.11$, (c) upstream at $\lambda = 42.16$ and (d) downstream at $\lambda = 42.16$.

Fig. 9 presents the mode-frequency map for the MAP and modal acoustic pressure response functions together with their constituent components of $|(x_l^{\pm})_j K_{ji}^{-1} W_i|^2$, $|V_l^{\pm}|^2$ and power factor $\zeta_l^{\pm}$. Multiplication of the results in Fig. 9(a) and (b), denoting the mode-frequency maps, respectively, for $|(x_l^{\pm})_j K_{ji}^{-1} W_i|^2$ and $|V_l^{\pm}|^2$, leads to the results in Fig. 9(c) representing the modal acoustic pressure, $R_l^{\pm}$. As described in Fig. 8, the component, $|(x_l^{\pm})_j K_{ji}^{-1} W_i|^2$, is found to determine the detailed shape of the mode-frequency map for the MAP and modal acoustic pressure except for the modes around the minimal modal lines determined by the component $|V_l^{\pm}|^2$. The magnitude of the acoustic pressure modes near cut-off is large due to the behavior of $|V_l^{\pm}|^2$. Multiplication of the results in Fig. 9(d) denoting the power factor $\zeta_l^{\pm}$ with the results in Fig. 9(c) produces the MAP response function $Q_l^{\pm}$. As described in Fig. 8, this power factor term implies that the relative magnitude of modes near the cut-off are diminished in both directions, and that the magnitude of the modes in the middle range away from the cut-off modes at given frequencies make a large contribution to

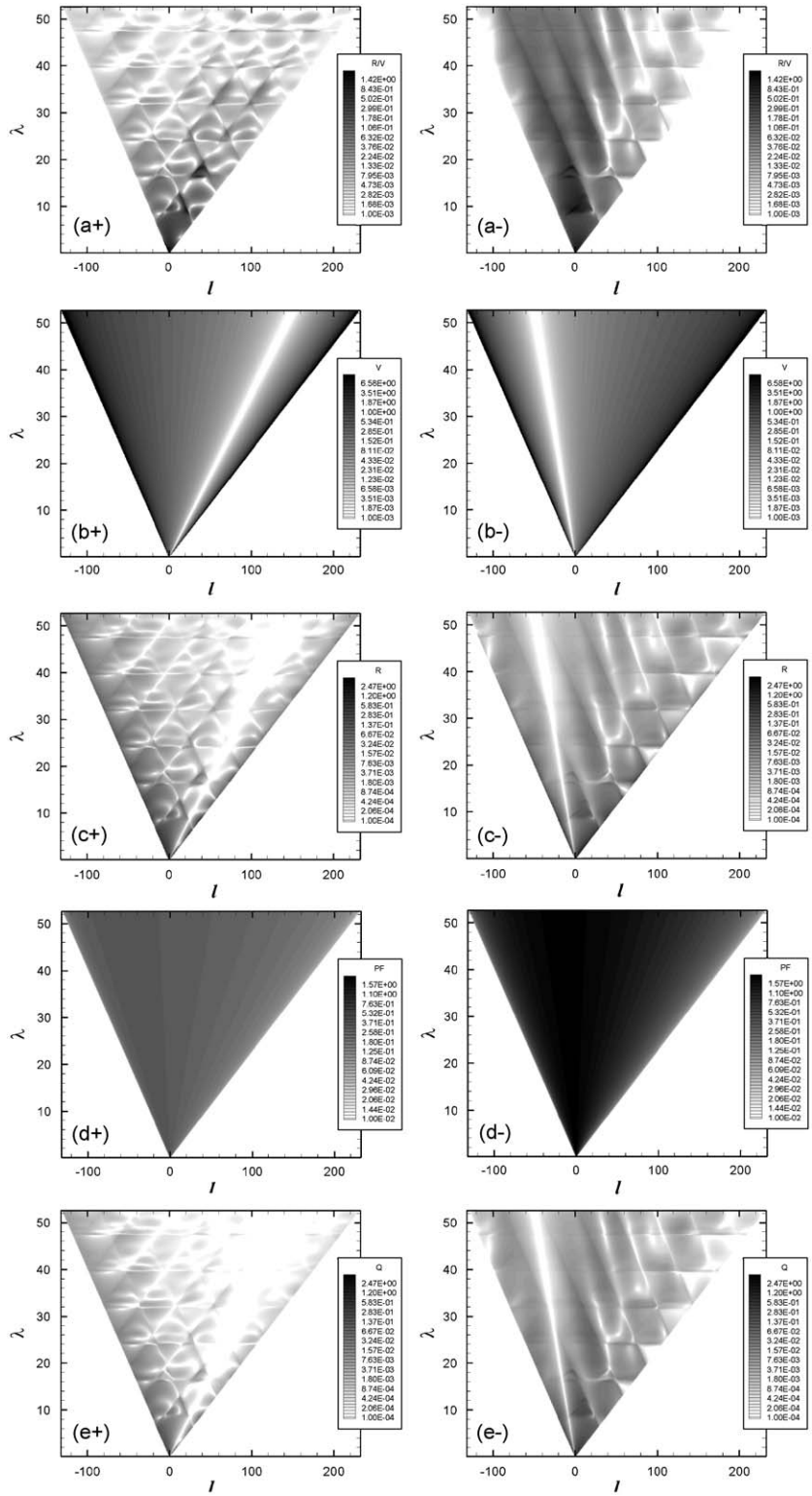

Fig. 9. Decomposition of modal acoustic power: (a) $|(x_l^{\pm})_j K_{ji}^{-1} W_i|^2$, (b) $|V_l^{\pm}|^2$, (c) $|R_l^{\pm}|$, (d) $|\zeta_l^{\pm}|$ and (e) $|Q_l^{\pm}|$ (left figures denote the upstream and right figures denote the downstream).

the total acoustic power in the downstream direction while those near cut-off make a larger contribution in the upstream direction.

5. Conclusion

The MAP radiated by a cascade of flat-plate airfoils interacting with homogeneous, isotropic turbulence has been investigated. The total acoustic power is expressed as the sum of the sound powers due to a finite number of cut-on acoustic modes, each of which can be expressed as the product of three terms: a turbulence frequency-wavenumber distribution, an upstream or downstream power factor and an upstream or downstream acoustic response function. The effect of these terms in the MAP has been examined. For an isotropic turbulent gust, the turbulent term is shown to reduce the MAP without significant change of its distribution. It is shown that, for subsonic flow, modal lines of minimum sound power exist in the upstream and downstream mode-frequency maps for MAP, which are determined by the transfer factor $|V_l^{\pm}|^2$ from the bound vortex on a flat airfoil to the modal acoustic pressure in the acoustic response function. The downstream power factor tends to increase the MAP away from cut-off while the upstream power factor is likely to decrease the MAP. The modes close to cut-off decreases strongly due to the behavior of the power factor. The modes close to cut-off, therefore, do not contribute strongly to the radiated acoustic power in the downstream direction, although the modal acoustic pressure is high for these modes. This result may imply that different strategies are needed for the control of broadband noise due to cascade–turbulence interaction in the upstream and downstream directions.

Acknowledgment

This work was supported by the Korea Science and Engineering Foundation (KOSEF) grant funded by the Korea government (MEST) (No. R01-2007-000-10207-0).

References

[1] R.K. Amiet, Acoustic radiation from an airfoil in a turbulent stream, *Journal of Sound and Vibration* 41 (1975) 407–420.
[2] S. Kaji, T. Okazaki, Propagation of sound waves through a blade row II: analysis based on the acceleration potential method, *Journal of Sound and Vibration* 11 (1970) 355–375.
[3] S. Kaji, T. Okazaki, Generation of sound by a rotor stator interaction, *Journal of Sound and Vibration* 13 (1970) 281–307.
[4] S.N. Smith, Discrete frequency sound generation in axial flow turbomachines, Reports and Memoranda no. 3709, Aeronautical Research Council, 1972.
[5] D.S. Whitehead, Classical two-dimensional methods, in: M.F. Platzer, F.O. Carta (Eds.), *AGARD Manual on Aeroelasticity in Axial Flow Turbomachines*, *Unsteady Turbomachinery Aerodynamics* (*AGARD-AG*-298), Vol. 1, Neuilly sur Seine, France, 1987 (Chapter 3).
[6] R. Mani, G. Hovray, Sound transmission through blade rows, *Journal of sound and vibration* 12 (1971) 59–83.
[7] W. Koch, On transmission of sound through a blade row, *Journal of Sound and Vibration* 18 (1971) 111–128.
[8] N. Peake, The scattering of vorticity waves by an infinite cascade of flat plates in subsonic flow, *Wave Motion* 18 (1993) 255–271.
[9] N. Peake, The interaction between a high frequency gust and a blade row, *Journal of Fluid Mechanics* 241 (1992) 261–289.
[10] N. Peake, E.J. Kerschen, Uniform asymptotic approximation for high frequency unsteady cascade flow, *Proceeding of the Royal Society* 449 (1995) 177–186.
[11] S.A.L. Glegg, The response of a swept blade row to a three-dimensional gust, *Journal of Sound and Vibration* 227 (1999) 29–64.
[12] D.B. Hanson, K.P. Horan, Turbulence/cascade interaction: spectra of inflow, cascade response, and noise, AIAA-98-2319, 1998.
[13] D.B. Hanson, Theory for broadband noise of rotor and stator cascades with inhomogeneous inflow turbulence including effects of lean and sweep, NASA CR 2001-210762, 2001.
[14] C. Cheong, P. Joseph, S. Lee, High frequency formulation for the acoustic power spectrum due to cascade–turbulence interaction, *Journal of the Acoustical Society of America* 119 (2006) 108–122.
[15] V. Jurdic, An Investigation into Turbulence Cascade Interaction Noise, A Progress Report for a Ph.D., ISVR, University of Southampton, UK, 2006.
[16] C.R. Lowis, P. Joseph, Determining the strength of rotating broadband sources in ducts by inverse methods, *Journal of Sound and Vibration* 295 (3–5) (2006) 614–632.